CRITICAL FATIGUE AND QUASI-STATIC BEARING DAMAGES OF A PINNED JOINT IN BOTH $[0/\pm45/90]_{3S}$ AND $[90/\pm45/0]_{3S}$ CFRP LAMINATES

Satoshi Seike*, Yoshihiro Takao, Wen-Xue Wang, Terutake Matsubara **
***Kyushu University, Department of Aeronautics and Astronautics,**
****Kyushu University, Research Institute for Applied**

Keywords: *CFRP, pin joint, fatigue, damage mechanism*

Abstract

A mechanically fastened joint in Carbon Fiber Reinforced Plastic (CFRP) laminates is necessary due to its advantages in inspection, replacement and reliability. The mechanical joint should be designed to make the bearing failure mode occur because the strength is high and the joint fails non-catastrophically. This study detailed the bearing damage evolution of the pinned joints for both $[0/\pm45/90]_{3S}$ and $[90/\pm45/0]_{3S}$ CFRP laminates and its difference between static and fatigue loading is discussed. In static tests all 0° layers have kink at the maximum loading and the kink is a trigger to the final failure. On the other hand, under fatigue loading the final damages start mostly from collapse at the loaded surface edge. It is also found that delamination of fatigue case is longer than that of static and that $[90/\pm45/0]_{3S}$ presents higher strength and shorter delamination than $[0/\pm45/90]_{3S}$ in both static and fatigue cases.

1 Introduction

Carbon Fiber Reinforced Plastic (CFRP) that has high specific strength and stiffness has been widely used as secondary structures and will be as primary structures of various aircrafts. A mechanically fastened joint in CFRP laminates is necessary due to its advantages in inspection, replacement and reliability, even though it has disadvantage in stress concentration.

There are three macroscopic failure modes[1)-6)] as shown in Fig.1. They depend on the shape of CFRP mechanical joint specimen. In this study the bearing mode is focused on, since it has high strength and toughness, and a mechanical joint is designed to make it occur. Hart-Smith[7)] discussed the geometrical condition for bearing failure mode and requested both W/D and E/W to be more than 5, where W, D and E denote the specimen width, hole diameter, and the distance between end edge and hole center, respectively.

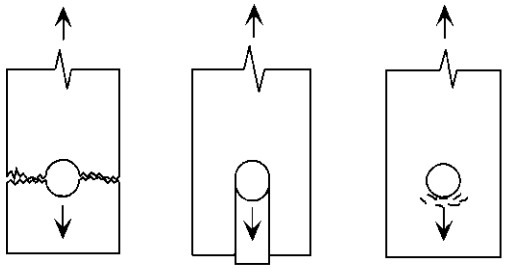

Fig. 1. Failure modes

There are many designed parameters such as stacking sequences, geometry, the number of pins, the material and the torque force of washers[8)-10)] and they were studied in static tests.

The failure mechanism of a joint was also investigated under static load. There are two main approaches to solve this complicated problem. One is a numerical simulation[11)] and the other is the microscopic investigation of damage evolution[4)10)12)]. Wang et al.[8)] reported the bearing failure of a pinned joint and attributed it to matrix cracks, delamination, fiber kink, and other factors. Camanho et al.[10)] conducted bolted joint tests and examined the evolution of three-dimensional microscopic damage in the tension, shear-out, and bearing modes. Furthermore, Hirano et al.[12)] reported the effect of temperature on the bearing mode failure of a pinned

joint and the following noticeable results at room temperature for both $[0/\pm45/90]_{3S}$ and $[90/\pm45/0]_{3S}$ CFRP laminates.

Fatigue tests for the mechanical joint of composite laminates were performed by Smith et al.[13] by using a bolted joint. It was presented that a bolt torque was an important parameter and damage evolution was small when the clamping force of the bolt was large. There are few studies about failure mechanism of fatigue. Thus, the damage evolution of a CFRP mechanical pinned joint is studied in the present paper and is discussed with reference to the static case.

In this study tensile fatigue tests of a pinned joint that is kind of a mechanical joint in CFRP and related studies are performed to obtain the failure mechanism. Firstly, a relation between load and cycle to failure is obtained. Next, the bearing damage of a specimen in fatigue tests is observed and the evolution as a function of cycle is clarified.

Though the detailed comprehensive study[12] has been performed under the static loading condition, the experimental study is performed again in this paper with the use of the same specimen as used in fatigue tests, that is, a practical full-circular-hole joint specimen since there is clear difference from the mechanical point of view between a half and full-circular-hole; the latter has a ligament part to support the axial load and the former does not; the fair and critical comparison between static and fatigue loading condition needs exactly the same condition except loading condition.

One more comment is added regarding the use of a pinned joint without clamping torque before closing this chapter. It is expected that the bolted joint with clamping torque should be used to obtain practical and useful technical information, and the future final goal is to obtain the difference and correspondence of failure mechanism of a bolted mechanical joint between the static and fatigue loading. However, the clamping torque with washer complicates the failure mechanism and conceals its intrinsic difference between fatigue and quasi-static loading with the probabilistic effect of friction due to clamping force as follows.

Clamping torque yields contact and friction between the specimen surface of CFRP and washer. Friction has three roles: distribution of force, unstableness of phenomena due to stick-slip process of sliding, and constraint of deformation due to friction force. Distribution of force decreases a load component applied to the critical damage, which increases the strength of the joint. Unstableness may conceal the difference of basic mechanism between static and fatigue failure. Constraint suppresses the deformation that is necessary for basic damage propagation and evolution and it is afraid that other damages might be activated and that damage evolution becomes much complicated. Effects of these unstableness and constraint are avoided in a pinned joint. Thus, a simple joint without clamping torque is adapted here and static and fatigue tests of a pinned joint with a full-circular-hole are performed to obtain the basic difference between both failure mechanisms of a joint, which is a key item of the present paper.

2 Bearing Test of a Mechanical Joint

2.1 Material and Specimen

The material used in this study was quasi-isotropic CF/Epoxy T800H/#3631 (Toray) laminates with the fiber volume fraction of about 60%. Stacked prepregs were cured by using an autoclave at 180°C and post-cured. The cured composite plate was cut into several pieces by using a diamond-tipped wheel saw with water as a coolant and a hole was drilled out. The specimen with the hole of 6mm in diameter is designed to have bearing failure and the hole is set 36mm away from an end edge along the center axis as shown in Fig.2, where W/D=E/D=6 and the 0° layer is aligned with the loading direction. During the drilling process, the specimen was sandwiched by two same used CFRP laminates to minimize the drilling damage around the circular hole. An undersized hole was first drilled out by a cemented carbide tool coated with diamond; then, finished with a cemented carbide reamer. After drilling, the finished surfaces of all specimens were inspected with an optical microscope and damaged ones were omitted. Two types of stacking sequences were prepared, namely, $[0/\pm45/90]_{3s}$ and $[90/\pm45/0]_{3s}$. Testing machine was MTS 810.21, and the jig and pin with a diameter of 6mm were made of SUS45C shown in Fig.3.

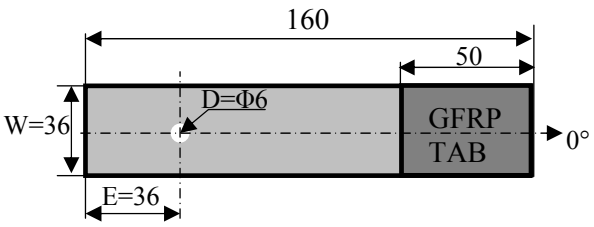

Fig. 2. Specimen geometry (mm)

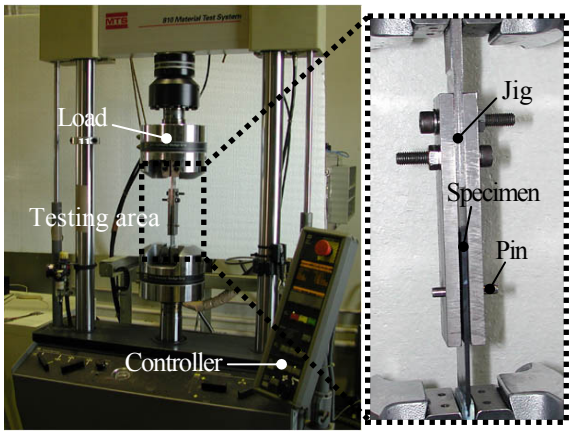

Fig. 3. MTS testing machine, jig and pin

2.2 Test Procedure

Load is applied to the specimen through a pin without clamping torque. Firstly, the static tensile test of full-circular-hole specimens was performed and an averaged ultimate tensile strength P_{UTS} of each laminate was obtained from the load-displacement curves by using a MTS testing machine. In the half-circular-hole specimen compressive load was applied and an averaged compressive strength P_{UCS} was obtained. Though the applied load is tensile this time, the expected damage is also due to the compressive load. Damage evolution was studied by the microscopic investigation at several loads. The specimen loaded to the prescribed load value is detached from the testing machine, a small piece including the bearing plane illustrated in Fig.4 is cut out of the specimen, the bearing plane is polished up into a mirror-like finish to present a clear image of internal damages, the damages are inspected in detail by an optical microscope of various magnifications, and the damage evolution under the static loading is obtained as a series of the cross sectional view of damages on the bearing plane including at 0.95 P_{UTS}, the maximum load P_{max} of each specimen and the final stage.

Next, the fatigue test of full-circular-hole specimens was performed with the maximum tensile load $P_{max,f}$ of $0.6P_{UTS}$, $0.7P_{UTS}$, $0.8P_{UTS}$ and $0.9P_{UTS}$ under the stress ratio R of 0.1 and the frequency of 10Hz, where R is defined as the ratio of the minimum load to maximum one and 10Hz is not high for the present pinned joint of CFRP laminates since the preliminary investigation did not present any serious difference of damage evolution between 1Hz and 10Hz. At first the S-N curves are obtained with the limit of 10^5 cycles. Secondly the specimen cyclically loaded to the prescribed cycles or elongation is detached from the machine and microscopic observation of the cross section was performed following the same procedure as in the static case. The value of elongation is set as the non-elastic elongation of 0.06mm, 0.1mm, 0.2mm and 0.3mm which will be explained in detail later.

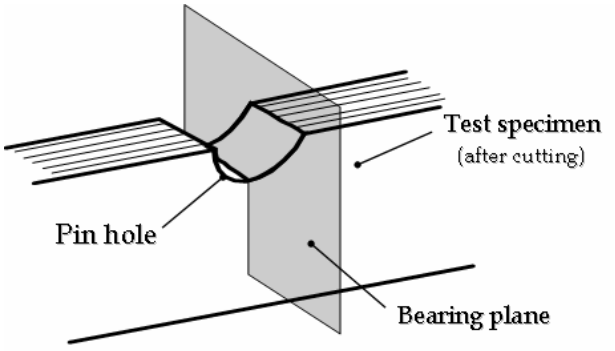

Fig. 4. Schematic view of bearing plane

3 Test Results and Discussions

3.1 Static Tests in Half-Circular Hole Specimen[12)]

The main results at room temperature by Hirano et al.[12)] are described first since they are closely related to the present study.

Static tests were performed with a half-circular-hole specimen by Hirano et al. The specimen has a free boundary perpendicular to the compressive loading direction in contrast to a practical full-circular-hole specimen that has the ligament part, that is, load path along the loading direction. Failure mechanism was studied by investigating cross sectional damages at several loads such as 60%, 80%, 90%, and 95% of the ultimate compressive strength P_{UCS} as well as to the maximum value P_{max} of an individual specimen and at the final stage, where P_{UCS} denotes the average value of each P_{max}. In a $[0/\pm45/90]_{3S}$ CFRP laminate, the delamination between surface 0° and 45° layer (at 0/45) could be observed at 0.95 P_{UTS} and the collapse of fibers in 0° layers at the loaded edge and matrix cracks in 45° and 90° layers were frequently detected but they were not and did not develop to a trigger to the final failure. The damage as a trigger to the final failure was a fiber kink at every inside 0° layer away from the loaded edge. The almost same kind of results were obtained in a $[90/\pm45/0]_{3S}$ CFRP laminate. Here it should be mentioned how to obtain the damage at P_{max} since additional ones usually overlap with objective ones at P_{max} due to the stored energy in loading fixtures. To prevent additional damages, a control code of MTS TestStarII™ was

used and the testing machine was programmed to be unloaded dynamically if the load decreased by 40 N from the previous load. The 40 N corresponded to 0.3% to 0.4% of the maximum load, and the load that was 40N less than the maximum load was considered to be the practical maximum load.

3.2 Static Tests in Full-Circular Hole Specimen

Representative load-displacement curves obtained from the static loading test are shown in Fig.5. They are divided into four parts as in the previous study[12] on the half-circular–hole compressive specimen: (Ⅰ) the first stage with the gradual increase of gradient, (Ⅱ) almost linear second stage, (Ⅲ) nonlinear third stage including a kind of yielding and the maximum load followed by a rapid drop of load, and (FS) final stage. The cross signs with an arrow in the figure denotes points such as $0.95P_{UTS}$, P_{max}, and the final stage where the detailed microscopic investigation is performed in a $[0/\pm45/90]_{3S}$ CFRP.

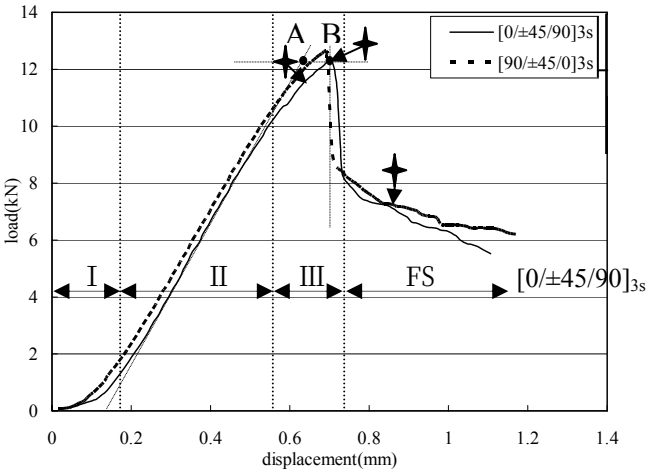

Fig. 5. Load-displacement curves under static loading

Firstly P_{UTS} is obtained as 12.0kN (σ= 0.3kN) and 12.3kN (σ= 0.6kN) in $[0/\pm45/90]_{3S}$ and $[90/\pm45/0]_{3S}$, respectively from nine specimens in each case, where two results of $[90/\pm45/0]_{3S}$ were not used since they showed premature failure due to the misalignment. The misalignment is related to the friction between a pin and hole edge of a CFRP laminate. Friction is originated mainly from the ligament part that has tensile axial force. The Poisson's effect of tension yields contraction on both width and thickness directions. On the other hand a pin supports axial compressive load and it tries to expand transversely. The contraction of a specimen and expansion of a pin lead to friction. As mentioned above friction has three roles that yield strength increase, unstableness and complication. The misalignment is supposed to be due to unstableness. Since the width and boundary condition are different, the direct comparison of strength is not possible between the present and previous results[12]. The σ in the parentheses denotes the standard deviation.

The damage at P_{max} is obtained by the same procedure developed by Hirano et al.[12] with a small modification in the value of 40N. The present full-circular-hole joint needs 60N instead of 40N probably due to the unstableness of friction to obtain the practical P_{max} steady; a testing machine is unloaded after the 60N decrease from P_{max}. This 60N is also very small compared to the maximum load of 12kN and about 0.5% of P_{max}. At this point the damage does not reach to the process of a rapid drop of load and the prompt unloading from 60N drop after P_{max} preserves almost the same damage as the one at P_{max}. The critical damage is revealed on the bearing plane after a careful polishing. The prompt response is important to suppress the appearance of additional damages.

Representative cross sectional views at $0.95P_{UTS}$, P_{max}, and final stage in $[0/\pm45/90]_{3s}$ are shown in Fig.6 (a)-(c), respectively, where the number of specimens is seven at each point. At $0.95P_{UTS}$ there are collapse (C) at the top of every 0° layer and delamination (D) at the 0/45 interface of the surface layer. This delamination corresponds to the longitudinal splitting on the surface.

At P_{max} there appear kink (K) at every inside 0° layer and delamination at every 0/45 interface. In the surface delamination which occurs at 0.95 P_{UTS} grows up to about 2mm. Delamination starts from each kink and collapse.

Both kink and collapse mean a kind of fiber buckling failure. Collapse occurs at the loaded surface edge and the transverse force originated from such as shear force or bending moment is supposed to contribute this damage. On the other hand kink occurs under pure compression at the 0° layer away from the contact surface and accompanies the intact or nearly intact zone between (collapsed) contact surface and itself. That is, kink is defined by this (nearly) intact zone. Otherwise the buckling is defined as collapse. Compared to the previous half-circular-hole joint, collapse appears

frequently. This is due to the rather severe friction related to the ligament part.

At the final stage many matrix cracks (M) start from kink and the shape of the final failure damage is a rather multiple-wedge type. In a half-circular-hole joint a single-wedge type was obtained in three out of five specimens. This difference is supposed to be related to the ligament as follows.

Splitting and surface layer delamination in a half-circular-hole joint in $[0/\pm45/90]_{3s}$ decrease the stiffness of surface region; this damaged joint expands because the weak surface can not suppress well the expansion being equal to damage propagation; the stress state of surface region becomes much more different from the inside one; the multi V-shape pattern is not expected. In $[90/\pm45/0]_{3s}$ there are no longitudinal splitting, a little transverse splitting and little surface layer delamination in a half-circular-hole joint at P_{max}; the fiber itself is intact even in the transversely split surface layer and makes surface region stiff and strong; this surface could suppress the expansion well, which is called as a band effect here; the stress state is rather similar through the thickness direction; every kink is expected to be a trigger to the final failure; the multi V-shape pattern is expected. It is also noted that the suppression of expansion makes friction force increase at the delaminated interface and is expected to block the delamination that is the main mechanism to reduce joint strength by separating laminates into slender plates with a low compressive resistance. This blocking could decelerate the development of damage from a single kink and present a multiple-wedge type damage.

The effect of ligament was described as the Poisson's effect through both width and thickness directions. The one through the thickness is discussed here. The contraction to the thickness direction gives compressive force to the peripheral area of the joint hole. This force could have the same effect on the damage evolution as the 90° surface layer in $[90/\pm45/0]_{3s}$ with a half-circular-hole joint. This band effect in a full-circular-hole joint makes the response in $[0/\pm45/90]_{3S}$ become similar to the one in $[90/\pm45/0]_{3S}$ and decreases the difference that was observed in the half-circular-hole joint. The difference of strength between $[0/\pm45/90]_{3S}$ and $[90/\pm45/0]_{3S}$ is a little less than 3% that is about a half of a half-circular-hole joint case. This is an explicit result of the ligament part and a multiple-wedge type is expected as the final damage pattern. No single-wedge type is observed in a full-circular-hole joint.

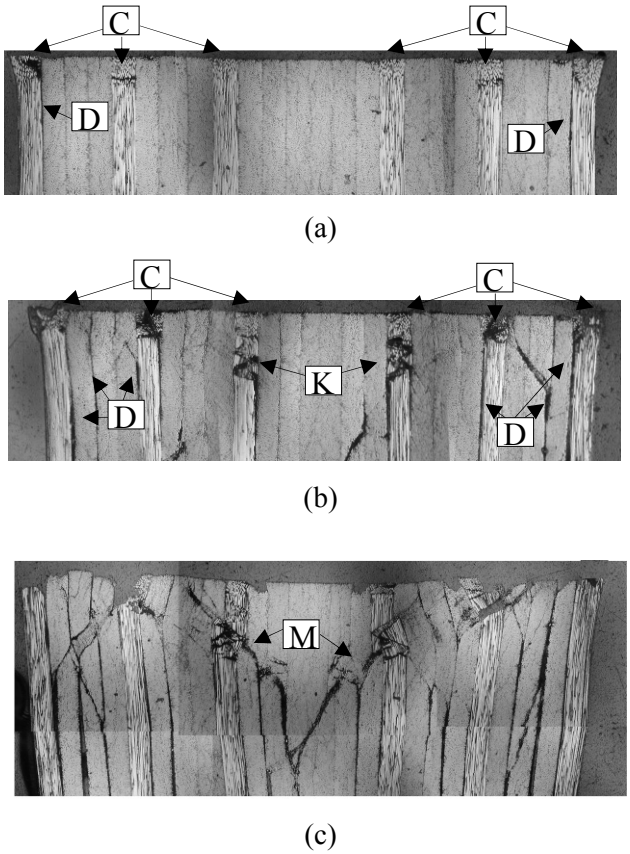

Fig. 6. Cross sections of $[0/\pm45/90]_{3s}$: (a) $0.95P_{UTS}$, (b) P_{max} and (c) final stage

In Fig.7 (a)-(c) the cross sectional views of $[90/\pm45/0]_{3s}$ are shown. The damage evolution is almost similar to that of $[0/\pm45/90]_{3S}$. Here different points are discussed. At $0.95P_{UTS}$ there is clear delamination at the 45/-45 interface than at the 90/45 of the surface because the difference of fiber direction is 90° and 45°, respectively. This delamination is detected as the swelling of the surface layer near the highly loaded hole edge. The swelling sometimes develops to an invisible transverse splitting to the naked eye at P_{max}. At P_{max} it can be mentioned that kink appears in the almost all 0° layers, since there is a rather intact zone between collapsed surface and kink. Delamination is also observed at most of 0/90 interfaces that have the difference of fiber direction of 90°. At the final stage matrix cracks develop from every kink of 0° layers and multiple-wedges composed of matrix cracks are formed up. The number of effectively developed delamination is smaller than $[0/\pm45/90]_{3S}$ case. This is explained by the band effect of surface layer.

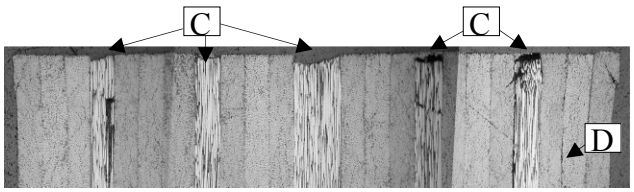

(a)

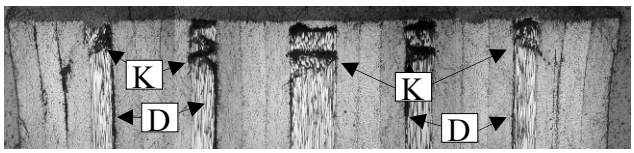

(b)

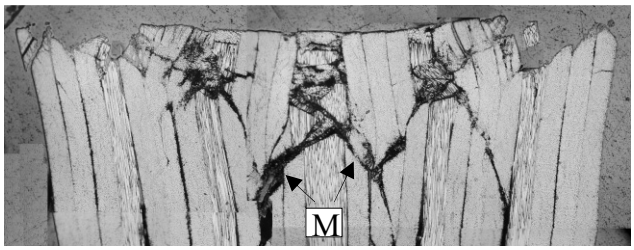

(c)

Fig. 7. Cross sections of $[90/\pm45/0]_{3s}$: (a) $0.95P_{UTS}$, (b) P_{max} and (c) final stage

3.2 Fatigue Tests

The relationship between load and fatigue life is obtained from three specimens at each condition as shown in Fig.8. The way how to assess fatigue failure will be touched later in Fig.9. The $[90/\pm45/0]_{3s}$ has higher strength than $[0/\pm45/90]_{3s}$ and this tendency can be explained by the band effect of surface layer as explained in Fig.8 (a): the 90° surface layer with intact fibers suppresses the expansion through the thickness direction, that is, the damage evolution as in the static case. Fig.8 (b) shows the relation between load normalized by P_{UTS} and cycle. Their points are on the same line. No fatigue failure appears at $P_{max.f}=0.6P_{UTS}$. Thus, the microscopic examination is performed for both $P_{max.f}$=8.4kN and 9.6kN.

Cyclic load-displacement curves at $P_{max.f}$ =8.4kN of $[0/\pm45/90]_{3s}$ and $P_{max.f}$=9.6kN of $[90/\pm45/0]_{3s}$ are shown in Fig.9 (a) and (b), respectively. They are obtained at 1, 10, 10^2, 10^3 and 10^4, and 5 cycles before failure. A straight line is drawn between points of the minimum and maximum load at the first cycle. A point of intersection of this straight line and horizontal axis is set as the origin of the figure, which neglects the first nonlinear stage in Fig.5. Three more lines are drawn parallel to and horizontally away by 0.06mm, 0.1mm and 0.2mm or 0.3mm from the first line. Points of intersection of these lines at $P_{max.f}$ in Fig.9 define non-elastic elongatins $U_{max.fd}$ of 0.06mm, 0.1mm and 0.2mm or 0.3mm at $P_{max.f}$ in each figure. The left one corresponds to $P_{max.f}$ at $N=10^3$ cycles. Others do to $U_{max.fd}$=0.06mm, 0.1mm and 0.2mm or 0.3mm at $P_{max.f}$. Microscopic investigation of the bearing plane is performed at these four points after being detached from the testing machine and inspected by the same procedure as in the static case.

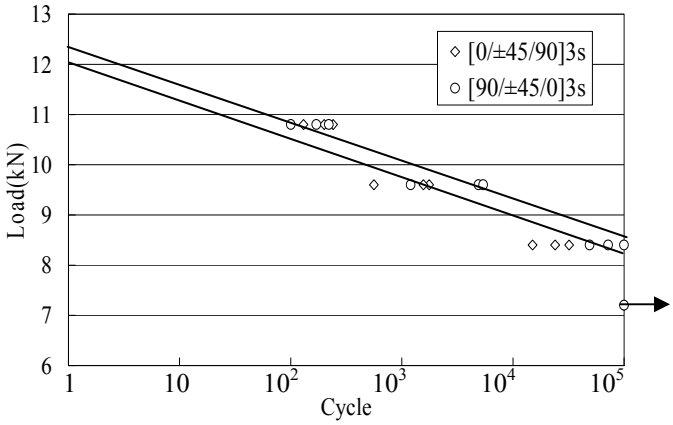

(a)

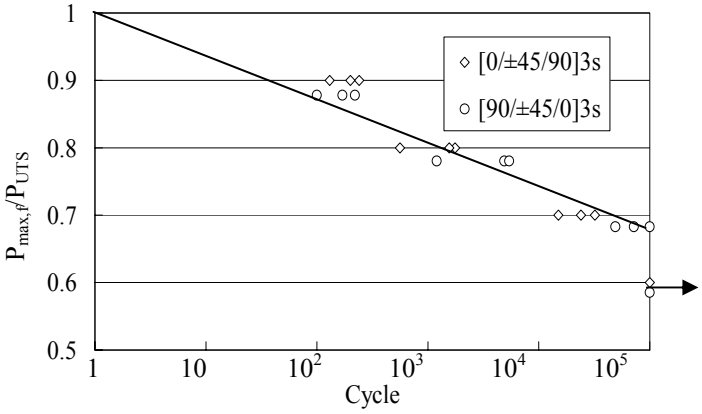

(b)

Fig. 8. The comparison of strength in two laminates: (a) Load-cycle, (b) $P_{max,f}/P_{UTS}$-cycle

The curve in Fig.9 moves gradually to the loading direction first and the moving speed increases near the failure. Fatigue failure is roughly assessed by this change of speed as shown in Fig.10. The speed increases drastically at around 0.06mm

non-elastic elongation and the final failure occurs at around 0.1mm non-elastic elongation.

The same amount of non-elastic deformation of about 0.06mm is noted in Fig.5. At the point of A, a straight tangent line of the stageIII in $[0/\pm45/90]_{3s}$ intersects with a line passing through the maximum load point P_{max} of B. The distance of AB is about 0.06mm and means the non-elastic deformation that appears at P_{max}. The $U_{max.fd}$ of 0.06mm might be a common critical value for both static and fatigue failures. The change of moving speed of cyclic curve will be studied in detail near future.

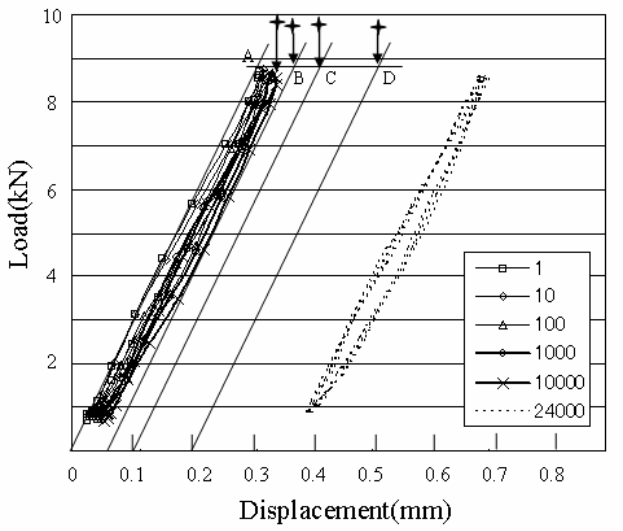

(a)

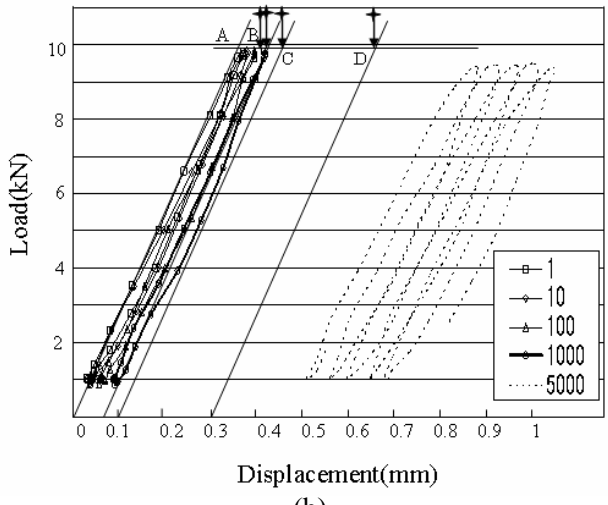

(b)

Fig. 9. Relation between load and displacement: (a) $[0/\pm45/90]_{3s}$, (b) $[90/\pm45/0]_{3s}$

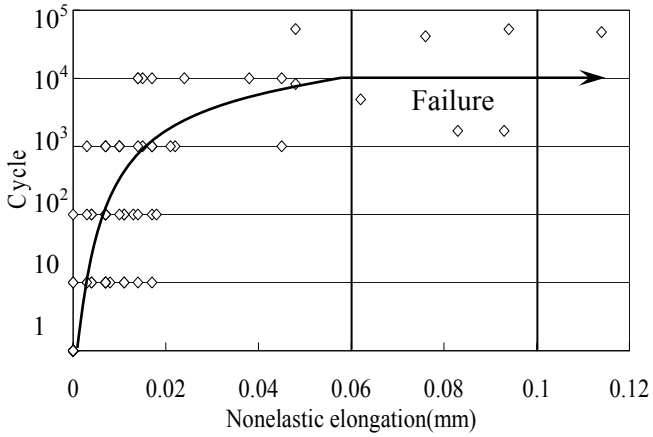

(a)

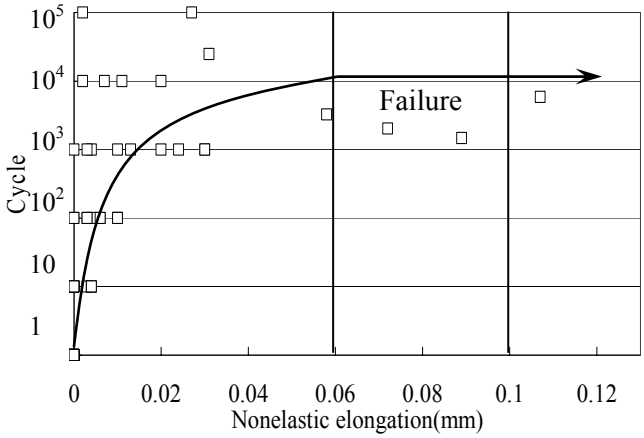

(b)

Fig. 10. Relation between cycle and nonelastic elongation: (a) $[0/\pm45/90]_{3s}$, (b) $[90/\pm45/0]_{3s}$

Cross sections of $0.7P_{UTS}$ in $[0/\pm45/90]_{3s}$ at 10^3 cycles, $U_{max.fd}$ of 0.06mm, 0.1mm and 0.2mm are shown in Fig.11 (a)-(d). At 10^3 cycles there are collapse at every 0° layer and delaminations at the 0/45 interface of the surface and at the next 45/-45 interface. Collapsed parts on the surface 0° layer are lost by the repeated comparatively large load due to the bending of a pin. The top edge of -45° layers is also lost during the preparation process of the cross section since the interface between fiber and matrix is deteriorated by repeated load. In 45° layers another edge of fiber is implanted deeply into the resin and it is not lost. It is noted that delamination is longer than the static case at this stage where neither matrix crack nor kink appears.

At $U_{max.fd}$ of 0.06 mm, delaminations at both 0/45 and 45/-45 interfaces develop and their number becomes almost double. A shear type matrix crack appears and develops from most of collapses, terminates at an interface and yields delamination.

Delamination appears directly from some collapses, too. Delamination is longer also at this stage where a shear type matrix crack appears.

At $U_{max.fd}$ 0.1mm and 0.2mm, delamination develops in length, width and especially the number. Shear type matrix cracks do, too and some cut through another 0° layer. Fig.11 (b) and (c) clearly show that the trigger to the final failure is not kink but collapse and that delamination develops much more than the static case.

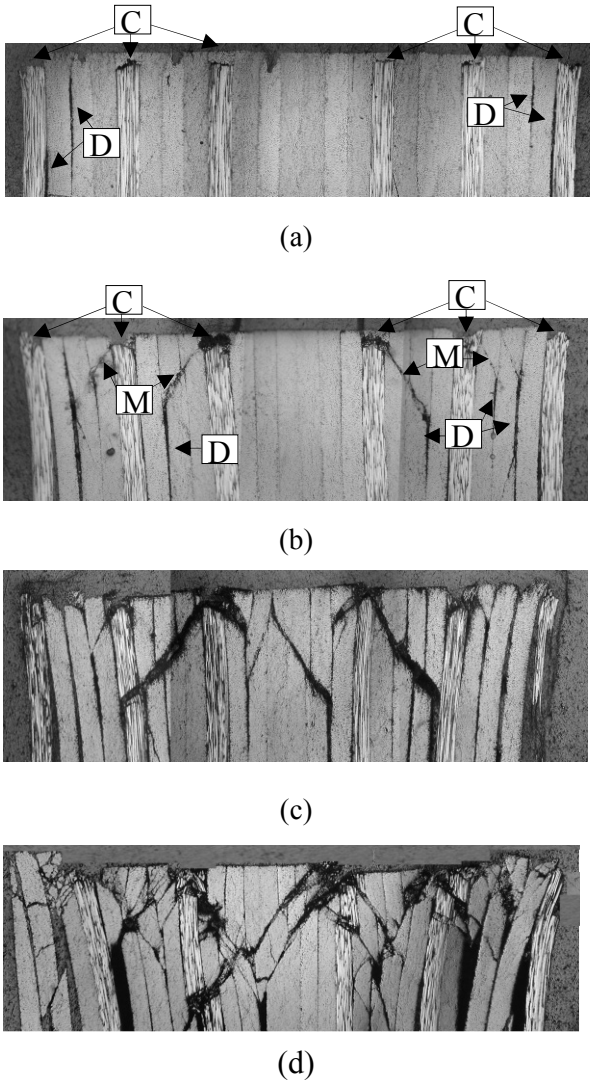

Fig. 11. Damage evolution of $0.7P_{UTS}$ in $[0/\pm45/90]_{3s}$: (a) 10^3 cycles, (b) non-elastic elongation of 0.06mm, (c) 0.1mm and (d) 0.2mm

Cross sections of $0.8P_{UTS}$ in $[90/\pm45/0]_{3s}$ are shown in Fig.12 (a)-(d). Here only the difference from Fig.11 is discussed. Fatigue life is more sensitive to the maximum load than stacking sequence as shown in Fig.8. This is true in the microscopic damage evolution and damages at $0.8P_{UTS}$ of $[90/\pm45/0]_{3s}$ develop more quickly than those at $0.7P_{UTS}$ of $[0/\pm45/90]_{3s}$. Though matrix cracks can be seen at the top of surface layer at 10^3 cycles, no delamination at 90/45 interface of the surface layer appears. This is a deceleration effect of the 90° surface on damage evolution as in the static case. Load increases to $0.8P_{UTS}$ leads to delamination in several interfaces of 0/90 and 45/-45 that have the difference of fiber angle of 90°.

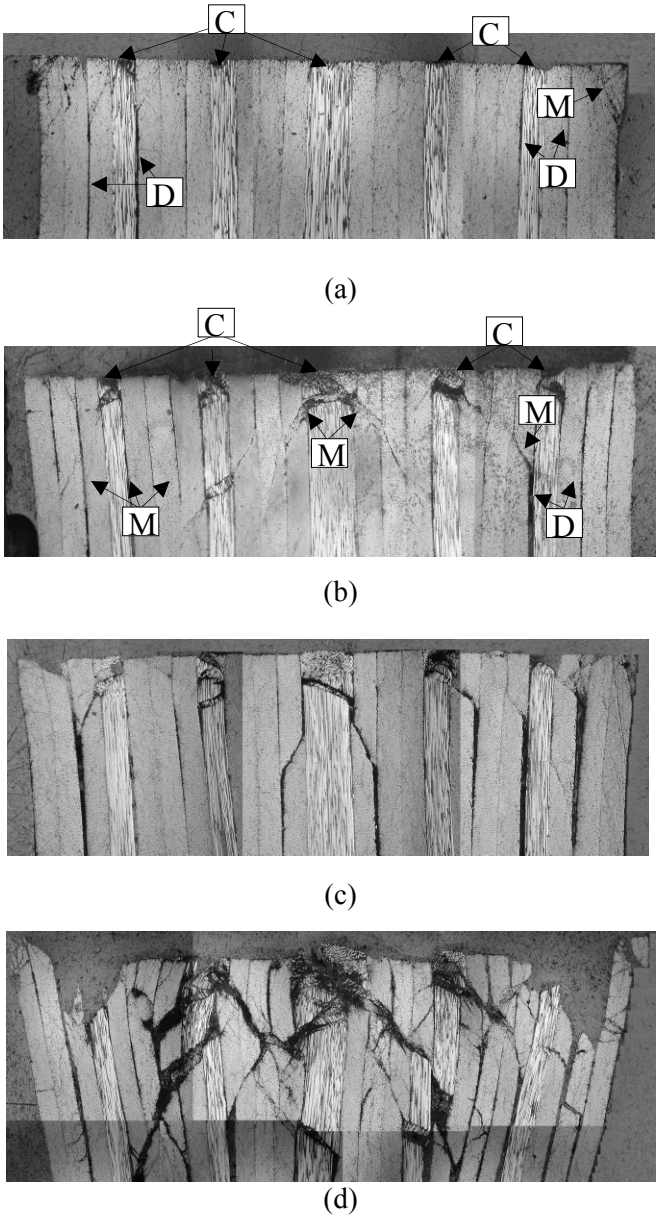

Fig. 12. Damage evolution of $0.8P_{UTS}$ in $[90/\pm45/0]_{3s}$: (a) 10^3 cycles, (b) non-elastic elongation of 0.06mm, (c) 0.1mm and (d) 0.3mm

At the $U_{max.fd}$ of 0.06 mm, delamination is observed in the almost all interfaces of 0/90 and 45/-45. In Fig.12 (c), the number and intensity of delamination are less than the $0.7P_{UTS}$ case of $[90/\pm45/0]_{3s}$ in Fig.11 (c) and no matrix crack cuts other 0° layer. Those are due to damage suppression by the surface layer. It should be noted that delaminations and matrix cracks develop also from collapses of 0° layers in both Fig.12 (c) and (d).

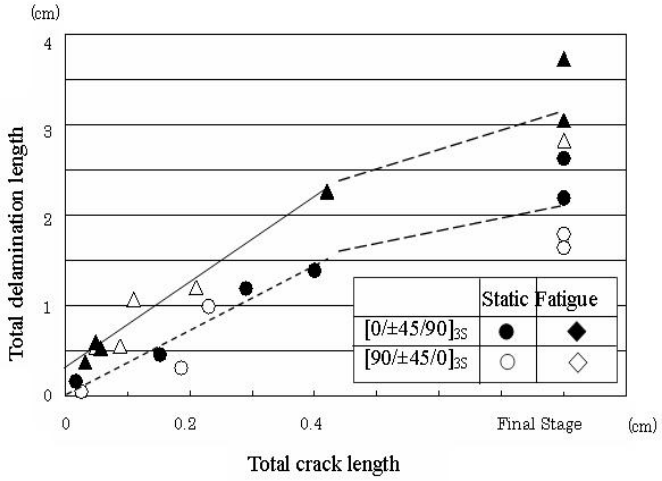

Fig. 13. Total delamination length in comparison with total matrix crack length under fatigue and static loading in $[0/\pm45/90]_{3s}$ and $[90/\pm45/0]_{3s}$

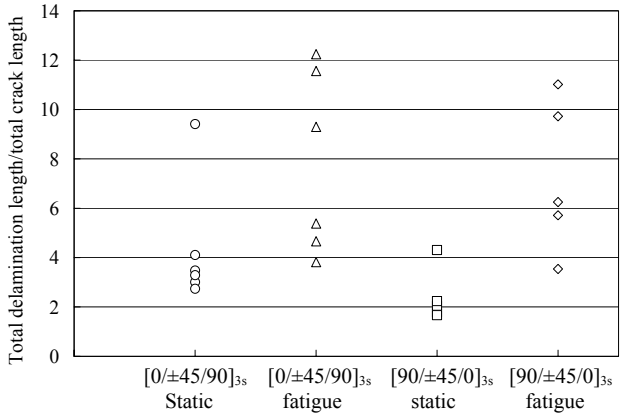

Fig. 14. The relation of total delamination length divided by total matrix crack length under fatigue and static loading in $[0/\pm45/90]_{3s}$ and $[90/\pm45/0]_{3s}$

Fig.13 and Fig.14 show the increase of the total delamination length area function of total matrix crack length and its ratio, respectively, where matrix crack length includes both shear crack and kink. The ratio of delamination to matrix crack in fatigue and $[0/\pm45/90]_{3s}$ is higher than in static test and $[90/\pm45/0]_{3s}$, respectively. In fatigue cases the maximum load $P_{max,f}$ is not high enough to yield kink directly and therefore delamination due to collapse starts before the matrix crack that starts from kink appears. The kink-like collapse that is driven by the misaligned compressive force always accompanies delamination. These are main reasons to increase delamination in fatigue cases.

4 Conclusions

The following results were obtained from quasi-static and fatigue tests on a pinned joint in CFRP laminates.

1. The reduction of the strength by cyclic loading is obtained. The strength of $[90/\pm45/0]_{3S}$ is higher than that of $[0/\pm45/90]_{3S}$ in the fatigue test as in the static case.
2. The above is explained by the band effect of intact 90° fibers in the surface layer.
3. The cyclic load–displacement curve moves to the loading direction with cyclic number increasing. The moving speed increases near the failure at about 0.06mm non-elastic elongation.
4. Delamination and collapse appear first under fatigue loading. Next, shear type matrix cracks start from the collapse.
5. The trigger to the final failure is collapse in fatigue though it is kink in quasi-static case.
6. The delamination in fatigue is longer than the quasi-static case.

Acknowledgements

This work was supported by the Ministry of Education, Culture, Sports, Science and Technology of Japan under a grant-in-aid (B-No.18360407) for Scientific Research.

References

[1] W.J.Quinn and F.L.Matthews, "*The Effect of Stacking Sequence on the Pin-Bearing Strength in Grass Fibre Reinforced Plastic*", Journal of Composite Materials, Vol.11, No.4, pp.139-145, 1977.

[2] D.Liu, B.B.Raju and J.You, "*Thickness Effects on Pinned Joints for Composites*", Journal of Composite Materials, Vol.33, No.1, pp.2-21, 1999.

[3] T.Ireman, T.Ranvik and I.Eriksson, "*On damage development in mechanically fastened composite laminates*", Composite Structures, Vol.49, No.2, pp.151-171, 2000.

[4] H.S.Wang, C.L.Hung and F.K.Chang, "*Bearing Failure of Bolted Composite Joints. Part I: Experimental Characterization*", Journal of Composite Materials, Vol.30, No.8, pp.1284-1313, 1996.

[5] P.S.Wu and C.T.Sun, "*Bearing Failure in Pin Contact of Composite Laminates*", AIAA Journal, Vol.36, No.11, 1998.
[6] Yi Xiao and Takashi Ishikawa, "*Bearing strength and failure behavior of bolted composite joints (part I: Experimental investigation)*", Composites Science and Technology, Vol.65, No.7-8, pp.1022-1031, 2005.
[7] J.Hart-Smith : "*Joining Fibre-Reinforced Plastics*" Elsevier Applied Science Publishers LTD, F.L. Matthews ed.,1987.
[8] I.Eriksson, "*the Bearing Strength of Bolted Graphite/Epoxy Laminates*", Journal of Composite Materials, Vol.24, No12, pp.1246-1269, 1990.
[9] P.A.Smith, M.F. Ashby and K.J.Pascoe, "*Modeling Clamp-Up Effects in Composite Bolted Joints*", Journal of Composite Materials, Vol.21, pp.878-897, 1987.
[10] P.P.Camanho and F.L.Matthews, "*Failure Mechanisms in Bolted CFRP*", Journal of Reinforced Plastics and Composites, Vol.17, No.3, pp.205-233, 1998.
[11] H.T. Sun, F.K. Chang, and X. Qing, "*The Response of Composite Joints with Bolt-Clamping Loads, Part I: Model Development*", Journal of Composite Materials, Vol.36, No.1, pp.47–67, 2002.
[12] N.Hirano, Y.Takao, and Wen-Xue Wang, "*Effects of temperature on the bearing strength of CF/Epoxy pinned joints*", Journal of Composite Materials, Vol.41, No.2, pp.335-351, 2007.
[13] P.A.Smith and K.J.Pascoe, "*Fatigue of Bolted Joints in (0/90) CFRP Laminates*", Composite Science Technology, Vol.29, No.1, pp.45-69, 1987.